SSRG International Journal of Mechanical Engineering
ISSN: 2348 – 8360 / https://doi.org/10.14445/23488360/IJME-V9I3P102

Volume 9 Issue 3, 15-23, March 2022

Original Article

A Turbojet-Powered, High-Load Vertical Take-off and Landing Flight Platform

Wan Tang[1], Jiale Zheng[2], Xuerui Qi[3], Saixuan Chen[4]

[1,2,3,4]*School of Mechanical and Automotive Engineering, Shanghai University of Engineering Science, Shanghai, China.*

Received: 18 February 2022 Revised: 24 March 2022 Accepted: 26 March 2022 Published: 30 March 2022

Abstract *- In the paper, we propose a turbojet-powered vertical take-off and landing flight platform with high load performance for extreme terrain， which can be applied in the medical, marine, and military areas. The platform uses a matrix layout of four turbojet engines and a thrust vector control system to achieve smooth flight. The dynamics simulation model of the flight platform was also established to analyze the effect of airflow disturbance on its stability. We carried out the lightweight and streamlined shell design relying on the mainframe structure, which effectively applied the performance characteristics of the turbojet engine to the flight platform and ensured its high load performance and reliability. In addition, the flight platform is streamlined, integrated, and reliable and has a modular adjustable feature.*

Keywords *- Turbojet powered, High load, Vertical take-off and Landing flight platform.*

1. Introduction

Jet UAVs have developed rapidly in recent years and have many applications. However, most aircraft can only meet the characteristics of being lightweight and fast. With the frequent and sudden occurrence of natural disasters, land rescue has not met the rescue needs to the maximum extent. It is costly to send out many crewless aerial vehicles, and rotary-wing UAVs cannot perform rescue operations at high altitudes or in complex terrain environments. Therefore, the vertical take-off and landing flight platform with high load capacity and stability. It can quickly transfer the casualty with its excellent balance performance, giving it maximum comfort to avoid secondary injuries. With their excellent manoeuvrability and flexibility in terrain surveys, jet drones can take off and land in relatively harsh environments, significantly improving safety. The flight platform is versatile due to the numerous mobile parts on modules that can be exclusively manufactured, dismantled, or supplanted; it can perform high-altitude aerodynamic horizontal flight and carry different types of up to 60kg load. In addition, with equipment installed on the flight platform, it is accessible environmental data from the survey site.

2. Structural Design Solutions

We seek to achieve the following four key points on our flight platform, which are the fundamentals of our modelling scheme.

- How to maximize the performance of the turbojet engine on the flight platform.
- How to overcome the shortage of strength in traditional structural design
- How to efficiently layout the vehicle and achieve lightweight.
- How to carry out attitude stability control of the flight platform.

2.1. Overall 3D Modeling of the Flight Platform

The internal frame structure of the flying platform was built first. We used hollow aluminium tubes to build the overall framework of the flight platform while using a matrix layout to place the energy and control systems. Thus, the structure can be divided on the Z-axis into a turbojet power layer, a frame support layer, and a landing support layer. [1]

Next, we model the installation of each layer. The engine is mounted on a fixed bracket and connected to the frame support layer using hollow aluminium tubes for the vortex jet power layer. Given that the flying platform needs to use the vortex jet airflow to obtain take-off power, we use servomechanism to adjust the rotation of the four nozzles for vector outflow. To efficiently use material and space, we attached the elbows to the landing support layer with bearings and bolted the landing support layer to the frame support layer. The role of the landing support layer (engine support frame) is to connect and support the vehicle's overall structure. The engine support frame and the engine mount are secured by bolts and reinforcements, while the bearings are embedded in the support frame and serve as the connection and transition, which plays a crucial role in attitude control [14].

In consideration of the high load operation of the flight platform, we lengthened and strengthened two support rods. It prevents the deformation of the flying platform and provides

the necessary guarantee for the manoeuvrability of the flying platform.

The whole flying platform adopts a modular design consisting of a frame module and four-engine support modules. The fuselage structure is shown in Figure 1, and the schematic diagram [2] of the whole aircraft model is shown in Figure 2.

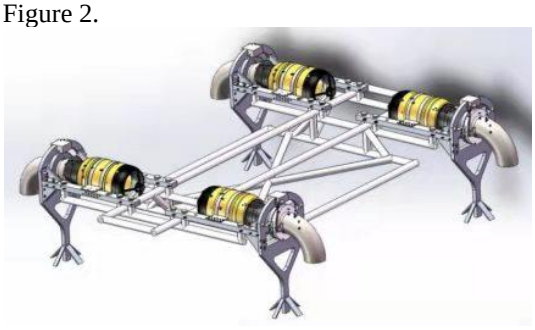

Fig. 1 Flight platform fuselage structure

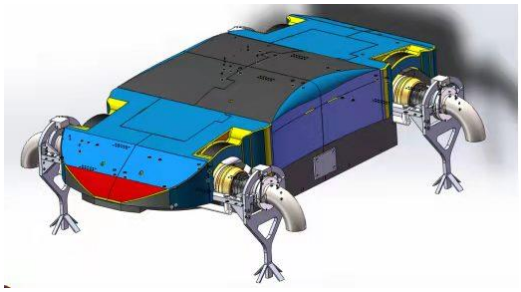

Fig. 2 Flight platform prototype

2.2. Engine Support Module Modeling

Our flight platform is powered by the Swiwin Xuan Yun micro turbojet engine. We found it hard to control the engine when placed vertically during engine ignition experiments, so we adopted a horizontal engine placement scheme. Finally, the engine nozzles are oriented outward, and the airflow is ejected through a 90° arc tube to provide power [15]. The arc tube is driven by servomechanism mounted on the engine mount （see Fig1）.

After determining the rudder shaft and arc nozzle, we conceptualized the rudder arm and connecting rod to form a four-link mechanism (see Fig 3).

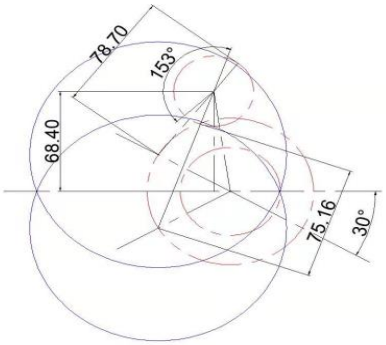

Fig. 3 Sketch of the four-link mechanism of the servo

The control system groups the four turbojet engines and can call different subroutines to switch to more flight modes. Using geometric methods, we arrived at a connecting rod length between 75.16 mm and 78.7 mm, so a reasonable length of 76 mm was chosen. The rudder can be rotated 180°, and the design requires a nozzle rotation angle of 30° front-to-back. Hence, the effective rotation angle of the rudder is 153°, with the remaining 27° as a margin for subsequent adjustment. Based on the characteristics of the diesel engine, we designed the front end of the nozzle in a flared shape to draw in enough air for the complete combustion of diesel fuel [3].

2.3. Internal Parts and Material Selection

Considering the flight platform's structural strength and weight, we chose the 6061 hollow aluminium tube as the main body of the flight platform, which significantly reduced the flight platform's mass. The turbojet power layer is made of 2AL2 aluminium alloy coated with high heat-resistant grade HRMB insulation material to prevent the nozzle flame's high temperature (above 600 degrees Celsius) from melting [17]. Careful material selection was required because the curved pipe directly contacted the vortex jet flame. After a comprehensive comparison, we chose 45 steel as the material for the arc pipe, which can withstand temperatures up to 800 degrees Celsius and sustained heat resistance up to 600 degrees Celsius [18].

3. Aerodynamic Simulation

In this paper, the aerodynamic study of the flying platform is based on the theory of automotive aerodynamics. After continuous trials and improvements, a featured outflow field simulation scheme was formulated. In the following paragraph， several characteristics of the fluid in the operating state of the flying platform are declared due to the need for subsequent studies.

3.1. Fundamentals of Fluid Mechanics

Viscosity is the interaction force within a fluid due to the microscopic relative motion occurring within the fluid, and any known fluid is viscous. In addition, viscous fluids can be divided into Newtonian and non-Newtonian fluids. When the rate of change of shear stress and velocity of a fluid satisfies Newton's law of internal friction, the fluid is said to be a Newtonian fluid. In addition, the fluid is a Newtonian fluid where the dynamic viscosity is constant. The dynamic viscosity of air is known to be constant, so the fluid studied in this paper, air, is a Newtonian fluid.

The gaps between fluid molecules exist, rendering all fluids compressible. However, fluid media with a Mach number less than 0.3 are usually considered incompressible [4]. The fluid studied in this paper has a very slight velocity, so it is deemed an incompressible flow. Its pressure field is specified implicitly through the continuity equation. A fluid is transient when its density, pressure, velocity, temperature, and

other parameters vary with time. In this paper, the velocity, density, and pressure of the air fluid studied do not vary with time, and, in addition, the effect of temperature can be neglected [4], making the air-fluid a constant flow.

The flow state of viscous fluids changes from time to time and is roughly divided into laminar and turbulent flow. Generally, it can be calculated by the Reynolds number formula. Distinguish between laminar and turbulent flow indicators is whether the Reynolds number reaches a critical value. The fluid flow state from laminar flow into turbulent flow when the corresponding Reynolds number for the upper critical Reynolds number, from turbulent flow into the laminar flow, when the corresponding Reynolds number for the lower critical Reynolds number.

The lower critical Reynolds number in engineering applications is generally considered 2320 [20]. If the Reynolds number of the fluid flow is greater than the lower critical Reynolds number, then the flow is said to be turbulent.

In summary, we calculate the characteristic parameters of the flight platform working conditions fluid, see Table 1.

Table 1. Characteristic parameters of the working fluid

Physical properties	Value	Units
Fluid Density	1.29	kg/m^3
Length of features	1.1	m
Dynamic viscosity	17.9×10^{-6}	$Pa \cdot s$
Average cross-sectional velocity	50	m/s
Reynolds number	3.96×10^6	N/A

3.2. Numerical Simulation of Outflow Field of Flight Platform

3.2.1. Pre-Processing

Due to the flight platform's irregularity, unprepared meshing will result in tremendous and low-quality generated meshes, which Fluent cannot simulate. Therefore, we simplified the shell model（see Fig4).

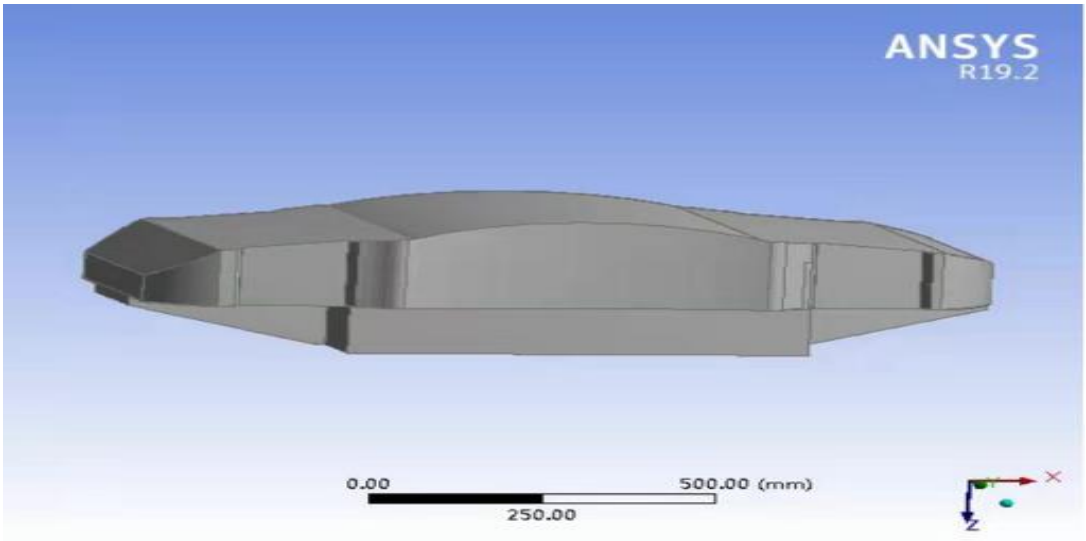

Fig. 4 Solid works model simplification of the flying platform

After the simplification, we select a so-called computational domain before the numerical simulation. The size of the computational domain is limited to the boundary of non-negligible disturbances to the flying platform, called the virtual wind tunnel. It was revealed that only experimental results with a wind tunnel blockage rate below 1% could ignore the errors arising from blockage disturbances [5]. Therefore, the blocking rate of the virtual wind tunnel is not less than 1% in this paper. The entrance area of the computational domain is calculated to be at least 71.14 m^2. Accordingly, we choose a rectangular fluid computational domain of 12 m in length, 8 m in width, and 4 m in height, with an entrance area of 96 m^2.

ANSYS DesignModeler can efficiently hybridize meshes [21]. This paper used a hybrid mesh strategy with good geometric adaptability and the ability to capture fluid flow details in the boundary layer. The surface of the flight platform is encrypted with triangular and quadrilateral meshes (see Fig 5), with a maximum size limit of 10 mm, and the computational domain is segmented into a hexahedron-dominated mesh. The final mesh results show a total mesh size of 330,000, with a quality higher than 0.79.

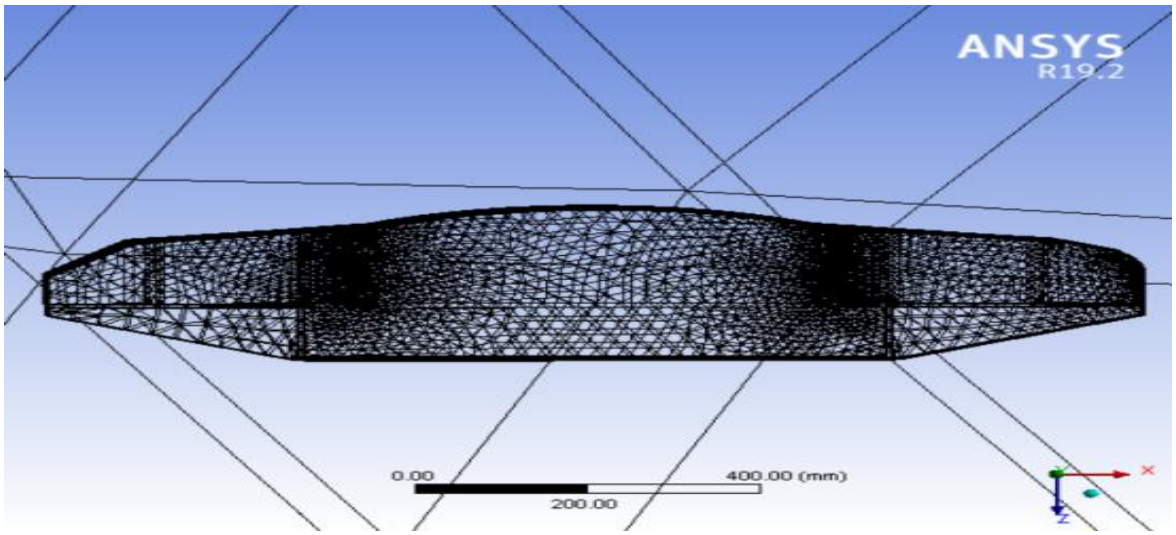

Fig. 5 Flight platform surface mesh

3.2.2. Determination of Boundary Conditions and Selection of Turbulence Model

Table 2. Boundary conditions and parameters

Boundary conditions and parameters	Types and values
Inlet boundary conditions	Speed inlet at 50m/s
Outlet boundary conditions	Pressure outlet, gauge pressure is 0
Wall boundary conditions	Shell Surface: non-slip wall; outside and top of calculation domain: slip wall
Computational Models	RNG k-epsilon Turbulence Model
Working temperature	*300K*

3.2.3. Simulation Results and Analysis

The residuals in the iterations converge to meet the accuracy requirements. K and epsilon equations converge faster than the continuity equation. At the same time, no backflow situation is generated in the calculation domain, which increases the accuracy of the calculation results. The aerodynamic drag coefficient monitored is 0.059.

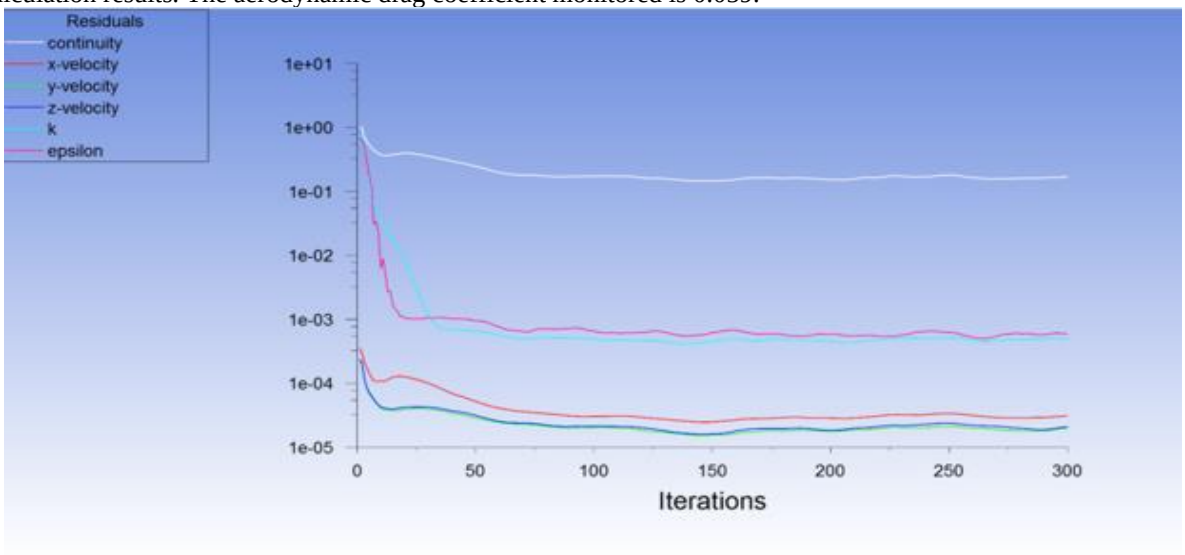

Fig. 6 Iterative calculation of residuals

According to Fig. 7 and Fig. 8, we can learn that the flight platform's head and lower bottom plate suffer high airflow pressure. In contrast, the upper and lower fuselage undergo lower airflow pressure. The airflow creates separation in these parts, causing an increase in their velocity and a decrease in pressure.

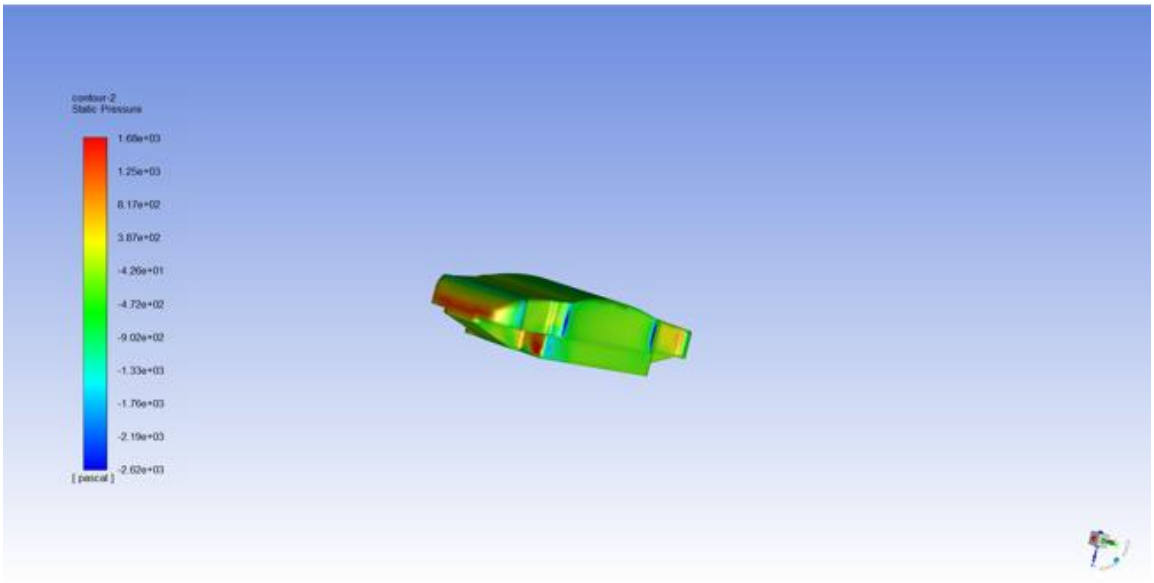

Fig. 7 Flight platform surface pressure contours

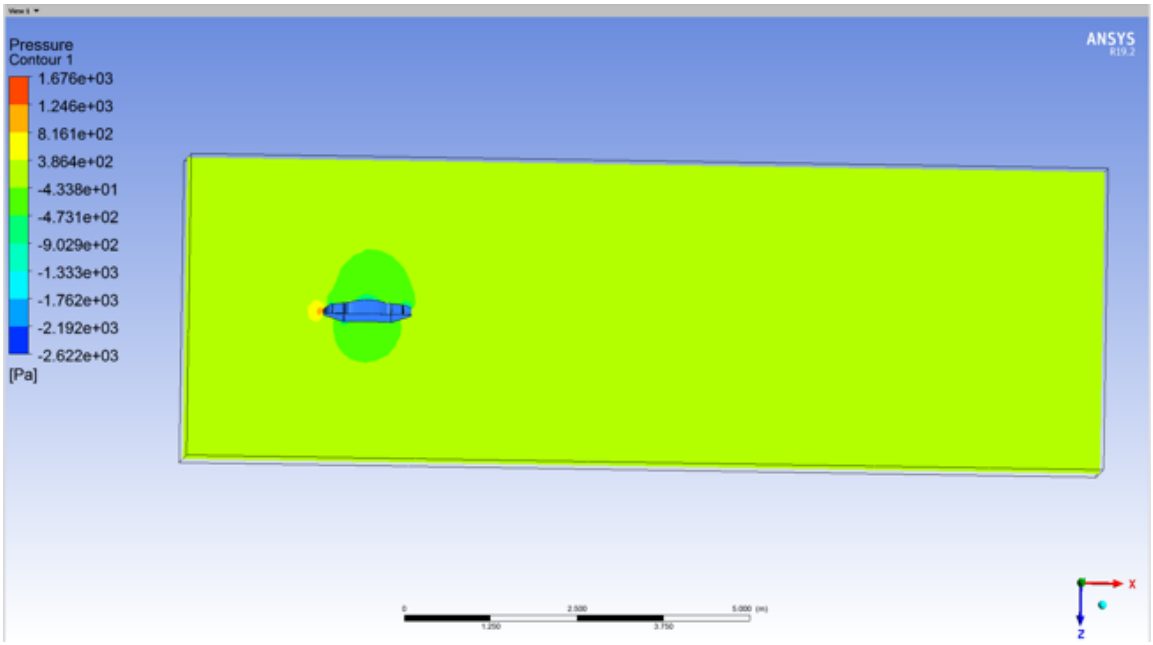

Fig. 8 Flight platform symmetry surface pressure contours

According to Fig. 8 and Fig. 9, inflow creates a stationary point at the front of the flight platform. As shown in Fig. 11, the incoming airflow is blocked at the head of the flight platform, causing its velocity to significant reduction, thus creating a branching airflow near the stationary point, creating a bypass airflow to the top and bottom of the fuselage. As a result, the pressure around this region is higher than the region unaffected by turbulent airflow， thus forming a positive high-pressure region.

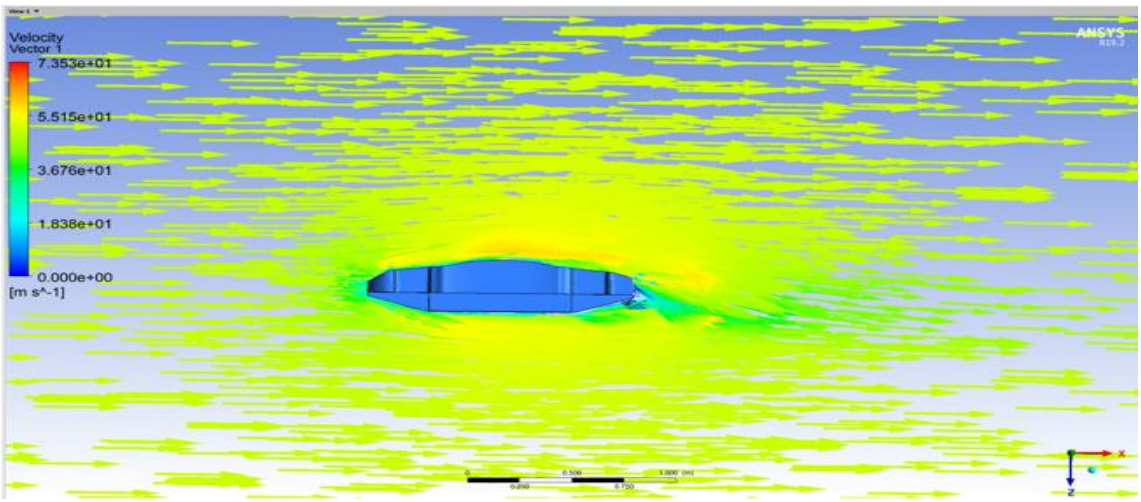

Fig. 9 Flight platform symmetry plane velocity vector

The airflow to the bottom of the fuselage is often too late to turn and separate as it passes through the high curvature "nose" of the fuselage head, creating a local low-pressure area. The high-velocity airflow to the roof above the fuselage re-establishes a low-pressure zone whose pressure distribution depends on the shape and curvature of the roof. At the rear of the roof, the gas flow gradually slows down, causing the pressure to tend to rise, creating conditions for airflow separation and the formation of a wake vortex, which in turn creates a large negative pressure zone at the junction of the roof and the rear of the vehicle. The symmetric surface velocity vector of the flight platform shown in Figure 9 formed two vortex zones at the front and rear ends of the flight platform, the former mainly due to the existence of significant airflow separation in this region and the latter due to the re-fusion of the two airflows around the upper and lower fuselages.

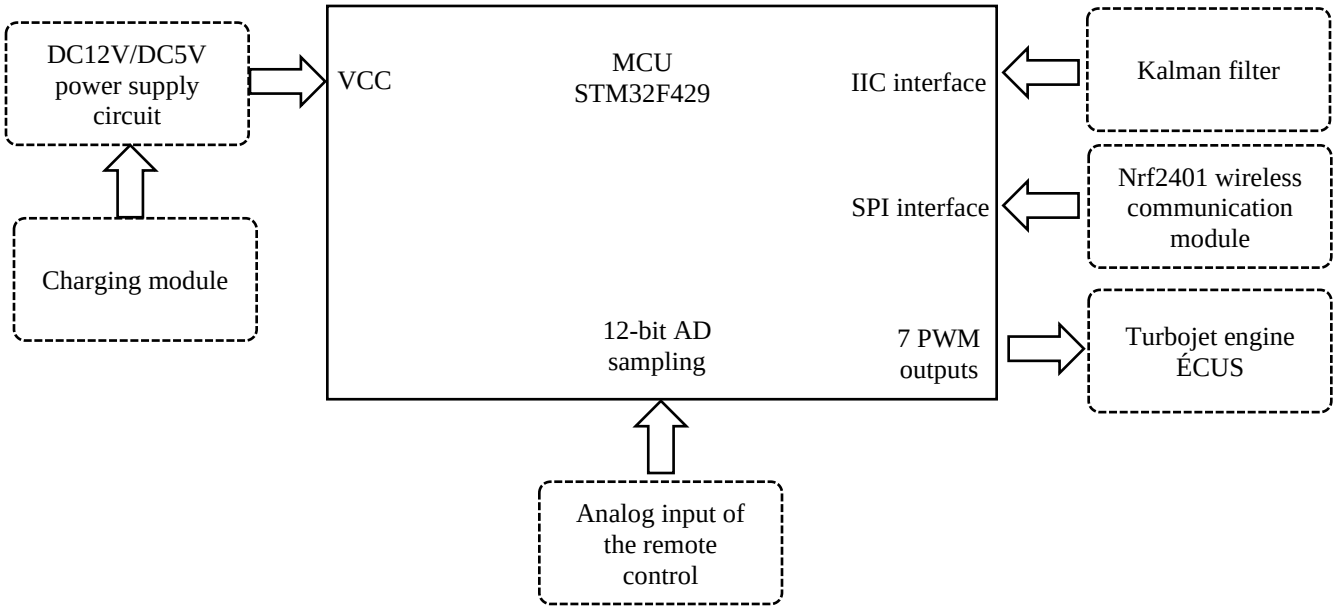

Fig. 10 Overall design of the flight control system

4. Fight Platform Control System

4.1. Overall Design of Plight Control System

The flight control system comprises six parts: the main control chip, the power module, the wireless communication module, the inertial guidance module, the turbojet engine ECU, and the remote-control module. The main control chip adopts STM32F429 [12]. The inertial guidance module adopts the MPU9250 attitude sensor and uses a Kalman filter and complementary filter for signal filtering to eliminate the effect of noise [7]. Then the filtered helpful information is

transmitted to the central control chip through the IIC interface. The wireless communication module liaises with the central control chip through the SPI interface. At the same time, the signals can be interchanged between the remote control and the main control chip through AD/DC conversion. The main control chip transmits PWM signals to the fuel pump for fuel supply control, which provides fuel to the power turbojet engine, thus realizing ignition, take-off, hovering, and landing. The overall design of the flight control system is shown in Figure 10.

4.2. Attitude Solving of Flight Control System

The attitude is the spatial position of the airframe, which is expressed by the heading angle φ, pitch angle θ, and cross-role angle γ. After determining the above three angles, the spatial position of the flight platform at a specific moment can be known. The MPU9250 sensor, which consists of a three-axis accelerometer, a three-axis gyroscope, and a three-axis magnetometer, is used to measure these three angles. The attitude control flow chart is shown in Figure 11.

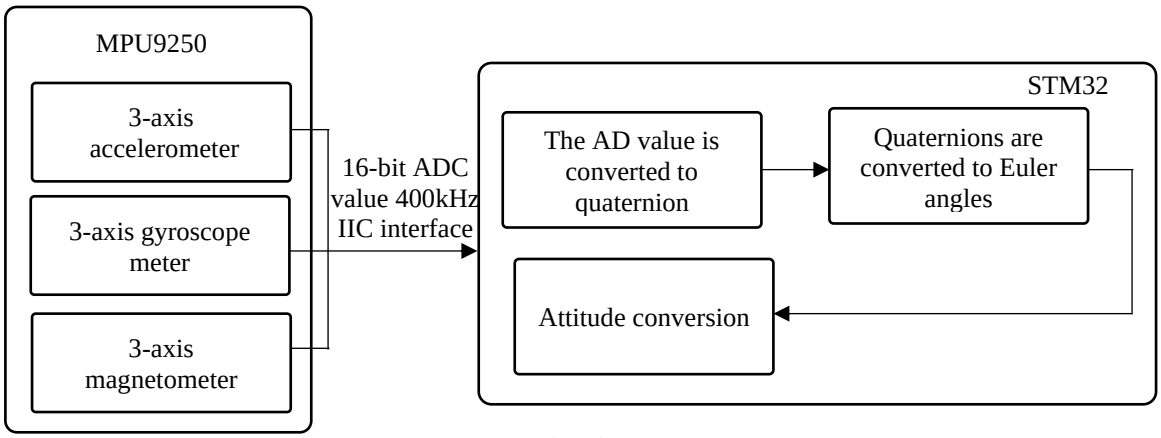

Fig. 11 Overall design of the flight control system

4.3. PID Design of Flight Control System

At the beginning of the study, we used a single-loop PID [8] to regulate the attitude angle of the flight platform. After processing, the single-loop PID system receives the desired angle and transmits the PWM signal to the turbojet engine through the STM32F429 chip to achieve a certain actual attitude angle. Then, we introduce negative feedback to transmit the error signal between the obtained actual attitude angle and the desired attitude angle to the PID system. Thus, the error is repeatedly calculated, and the updated signal is continuously transmitted to the turbojet engine, enabling the real-time adjustment of the attitude angle.

However, we found that the angular error alone could not be processed in practice. Otherwise, it would induce vibration of the flight platform or even an extremely tilted attitude. Therefore, we adopt an additional error processing of angular velocity.

Subsequently, we bring the angular velocity PID to the single-loop PID to form an inner and outer-loop PID. The angular velocity PID is used as the inner-loop PID, and the angular PID is the outer-loop PID [10]， as shown in Figure 12.

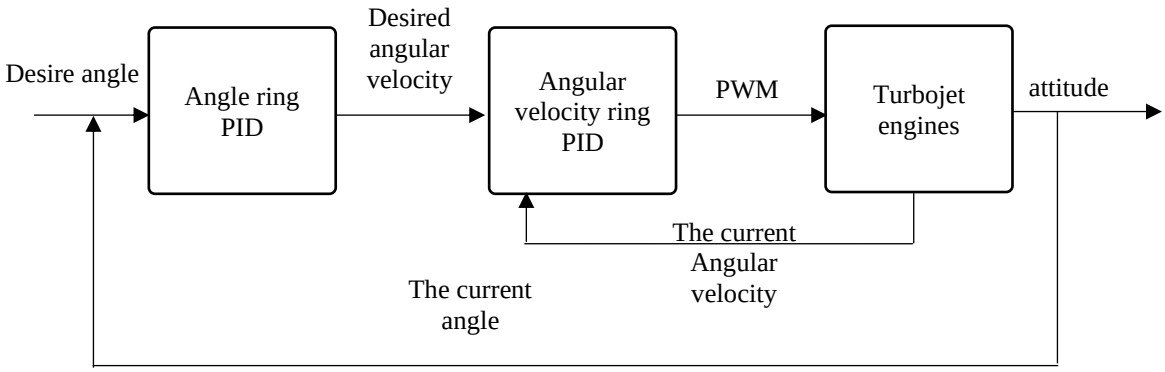

Fig. 12 String-level PID flow diagram

After calculating the ideal parameters, the main control chip and the servos operate simultaneously to achieve the multidimensional motion of the flying platform. The STM32F429 chip transmits the PWM signal to the turbojet engine oil pump [11], which controls the engine operation; the rudder controls the four-link mechanism to realize the flight attitude adjustment.

5. Conclusion

In this paper, a turbojet-powered flight platform with high-load vertical take-off and landing is proposed for the dilemma that rotary-wing UAVs cannot adapt to complex terrain. The flight platform has a sophisticated structural design and can carry a load of 80 kg despite lightweight materials. The turbojet engine has a total thrust of 84 kg and can carry 60 kg considering other effects such as air resistance. In addition, the platform can adapt to diverse terrain under its stable structure. We have built an aerodynamic simulation model of the flight platform to verify the rationality and implementation capability of the flight platform structure. The flight control system adopts string-level PID to update the flight attitude in real-time for autonomous control, which ensures the smoothness of the flight. The flight platform has multiple potential applications in natural disasters, national security, and the military industry.

Acknowledgment

This work was supported by Emerging Engineering Education of Shanghai University of Engineering Science （x202018001） and Jiangsu's key Research & Development plan（BE2020082-3）.

References

[1] Yang Haitao, Turbojet Multicopter , China, vol. 2, no. 17, 2016.

[2] Hou Zhiqiang, Wang Yunliang, and Gao Yong, “Calculation and Analysis of Unmanned Aerial Vehicle Shape Layout Design and Aerodynamic Characteristics,” *Journal of Naval Aeronautical and Astronautical Engineering College*, vol. 4, 2011.

[3] Fan Kaigang et al., “Research on Binary Vector Nozzle Characteristics Based on Miniature Turbojet Engine,” *The 9th Chinese Aeronautical Society Youth Science and Technology Forum*, 2020.

[4] Sun Wence, Engineering Fluid Dynamics-Second Edition, Dalian University of Technology Press, 1995.

[5] Zhang Yingchao, *Numerical Simulation Technology of Automobile Aerodynamics*, Peking University Press, 2011. [Google Scholar]

[6] Zhao Pengcheng, and Zhai Yan, “The Application and Development Trend of Turbojet Turbofan Engine in Uncrewed Aerial Vehicles[C]. Driven by Innovation,” *Accelerating the Development of Strategic Emerging Industries-Proceedings of the 7th Annual Conference of Science and Technology of Jilin Province*, pp. 295-296, 2012.

[7] Li Shilei, “Research on Quad-Rotor Aircraft Control System,” *Harbin Institute of Technology*, 2010.

[8] Yuan Sijie, “Research on Attitude Control of Quadcopter Based on PID Control,” *Digital World*, 2019.

[9] Guo Kang et al., “Research on Attitude Control of Quadcopter,” *Modern Computer*, vol. 27, no. 32, pp. 105-108, 2021.

[10] Sheng Guangrun, Gao Guowei, and Zhang Yingxue, “Cascade PID Control Under Rotor Interference of Quadrotor Based on STM32,” *Sensor World*, vol. 24, no. 11, pp. 32-37, 2018.

[11] Li Yang et al., “A Four-Rotor Control Method Based on Double-Ring PID Control,” *Fujian Computer*, vol. 34, no. 9, pp. 47-48, 2018.

[12] Zhang Dongsheng et al., “Design of Underwater Robot Control System Based on STM32F407,” *Proceedings of the 11th International Conference on Computer Engineering and Networks*, pp. 1216-1223, 2021. [CrossRef] [Google Scholar] [Publisher Link]

[13] Bai TingTing, Wang DaoBo, and Masood Rana Javed, “Formation Control of Quad-Rotor UAV Via PIO,” *Science China Technological Science*, vol. 65, pp. 432-439, 2022. [CrossRef] [Google Scholar] [Publisher Link]

[14] Q.X. Pang, “Design and Stability Control of Quadrotor Aircraft,” *He Fei: University of Science and Technology of China*, 2011.

[15] Pedro Castillo, Rogelio Lozano, and Alejandro Dzul, “Stabilization of a Mini Rotorcraft with Four Rotors,” *IEEE Control Systems Magazine*, vol. 25, no. 6, pp. 45-55, 2005. [Google Scholar]

[16] X.G. Cheng, The Design and Research of Quadrotor, Hang Zhou: Hangzhou Danzi University, 2012.

[17] J.F. Shi et al., “Review of Flight Tests for Multi-Layer Insulator Materials,” *Chinese Optics*, vol. 6, no. 4, pp. 457-469, 2013. [Google Scholar]

[18] K.D. Young, V.I. Utkin, and U. Ozguner, “Control Engineer's Guide to Sliding Mode Control,” *IEEE Transactions on Control Systems Technology*, vol. 7, no. 3, pp. 328-342, 1999. [CrossRef] [Google Scholar] [Publisher Link]

[19] Digvijay Kushawal et al., “Evaluation and Optimization of Cutting Parameters for Turning of En-8 Steel: A Taguchi Approach,” *International Journal of Mechanical Engineering (IJME)*, vol. 6, no. 4, pp. 35-44, 2017. [Google Scholar] [Publisher Link]

[20] Rahul Agrawal, and Dev Dutt Singh, “Simulation Study of Active Quarter Car Model Using Matlab and Simulink Software,” *SSRG International Journal of Mechanical Engineering*, vol. 7, no. 5, pp. 1-7, 2020. [CrossRef] [Publisher Link]

[21] Armin Yazdanshenas, and Chung-Hyun Goh, “Rockwell Hardness Testing on an Aluminum Specimen using Finite Element Analysis,” *SSRG International Journal of Mechanical Engineering*, vol. 7, no. 4, pp. 1-10, 2020. [CrossRef] [Google Scholar] [Publisher Link]

[22] Huong T.M. Nguyen, “Using Extended Kalman Filter to Observe State Parameters of the Twin Rotor MIMO System in Order to Install Model Predictive Control Algorithm Based Phisical Model,” *SSRG International Journal of Electrical and Electronics Engineering*, vol. 4, no. 12, pp. 1-7, 2017. [CrossRef] [Google Scholar] [Publisher Link]

[23] Shengjiang Yang et al., "New Integrated Guidance and Control of Homing Missiles with an Impact Angle against a Ground Target," *International Journal of Aerospace Engineering*, 2018. [CrossRef] [Google Scholar] [Publisher Link]

[24] Fang Yang-Wang et al., "Research Status and Development Trend of Guidance and Control of Aspirated Hypersonic Aircraft," *Journal of Aeronautics*, 2014.

[25] Yang Meng et al., "Design of Quadcopter Control System Based on STM32," *Microcomputers and Applications*, vol. 12, 2015.